JACS
JOURNAL OF THE AMERICAN CHEMICAL SOCIETY
Article
pubs.acs.org/JACS

Multimodal Polymer Nanoparticles with Combined ^{19}F Magnetic Resonance and Optical Detection for Tunable, Targeted, Multimodal Imaging *in Vivo*

Barbara E. Rolfe,[†] Idriss Blakey,[†,‡] Oliver Squires,[†] Hui Peng,[†] Nathan R. B. Boase,[†,‡] Cameron Alexander,[§] Peter G. Parsons,[⊥] Glen M. Boyle,[⊥] Andrew K. Whittaker,[†,‡] and Kristofer J. Thurecht*[,†,‡]

[†]Australian Institute for Bioengineering and Nanotechnology and [‡]Centre for Advanced Imaging, The University of Queensland, St Lucia, Queensland 4072, Australia

[§]School of Pharmacy, The University of Nottingham, Nottingham NG7 2RD, United Kingdom

[⊥]Queensland Institute for Medical Research, The Royal Brisbane Hospital, Herston, Queensland 4006, Australia

Supporting Information

ABSTRACT: Understanding the complex nature of diseased tissue *in vivo* requires development of more advanced nanomedicines, where synthesis of multifunctional polymers combines imaging multimodality with a biocompatible, tunable, and functional nanomaterial carrier. Here we describe the development of polymeric nanoparticles for multimodal imaging of disease states *in vivo*. The nanoparticle design utilizes the abundant functionality and tunable physicochemical properties of synthetically robust polymeric systems to facilitate targeted imaging of tumors in mice. For the first time, high-resolution ^{19}F/^{1}H magnetic resonance imaging is combined with sensitive and versatile fluorescence imaging in a polymeric material for *in vivo* detection of tumors. We highlight how control over the chemistry during synthesis allows manipulation of nanoparticle size and function and can lead to very high targeting efficiency to B16 melanoma cells, both *in vitro* and *in vivo*. Importantly, the combination of imaging modalities within a polymeric nanoparticle provides information on the tumor mass across various size scales *in vivo*, from millimeters down to tens of micrometers.

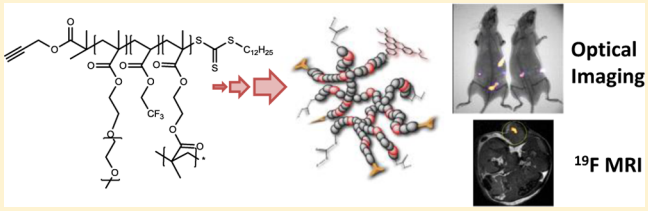

INTRODUCTION

In vivo molecular imaging has the potential to revolutionize modern medical diagnostics. Sensitive molecular probes with high signal-to-noise ratios that are capable of highly selective *in vivo* targeting are needed to probe biological processes, whether these are innate physiological processes or those resulting from a treatment or therapy.[1−3] The considerable challenges associated with achieving this goal stem from the fundamental problems associated with conventional imaging agents; for example, magnetic resonance imaging (MRI) often generates ambiguous assignments due to poor sensitivity, positron emission tomography (PET) suffers from relatively poor spatial resolution and radiation burden for the patient, and optical imaging techniques are hindered by tissue absorption of the radiation, making the technique inadequate for most deep-tissue analyses.[4,5] Significant advances in both materials science and imaging technology are thus required, with an urgent need for devices capable of utilizing multimodal imaging to enable sensitive and experimentally "orthogonal" detection modes and hence more definitive diagnosis of diseases. Combination of a highly sensitive modality (e.g., PET/optical) with a complementary modality that is highly specific and which exhibits exceptional spatial and anatomical resolution (e.g., MRI) is a potential means by which this step-change in imaging can be achieved.[6,7]

In order to be effective, molecular imaging agents must embody a number of important design features: they must primarily have a high imaging signal-to-noise ratio and be active in biological media; they must efficiently and actively target specific tissues, whether by direct means (receptor-mediated targeting) or indirectly (for example, via leaky vasculature[8]); and they must exhibit reliable pharmacokinetic/pharmacodynamic behavior, such that imaging performance is not compromised during lengthy imaging.[5,9] We accordingly focus our nanoparticle design on a hyperbranched polymer (HBP) scaffold,[10−13] employing a poly(ethylene glycol) (PEG)-based architecture to limit removal via the mononuclear phagocyte system (MPS),[14,15] while incorporating a branched architecture to endow multiple functionalities for attachment of both targeting ligands and complementary imaging modalities. Importantly for a biomedical application, adaptation of well-established chemistries to enable rapid and facile synthesis of the nanomaterials while retaining good control over the

Received: October 8, 2013
Published: January 17, 2014

   dx.doi.org/10.1021/ja410351h | *J. Am. Chem. Soc.* 2014, 136, 2413−2419

Scheme 1. Robust and Practical Approach for Synthesising Polymers with Controlled Size and Degree of Functionality[a]

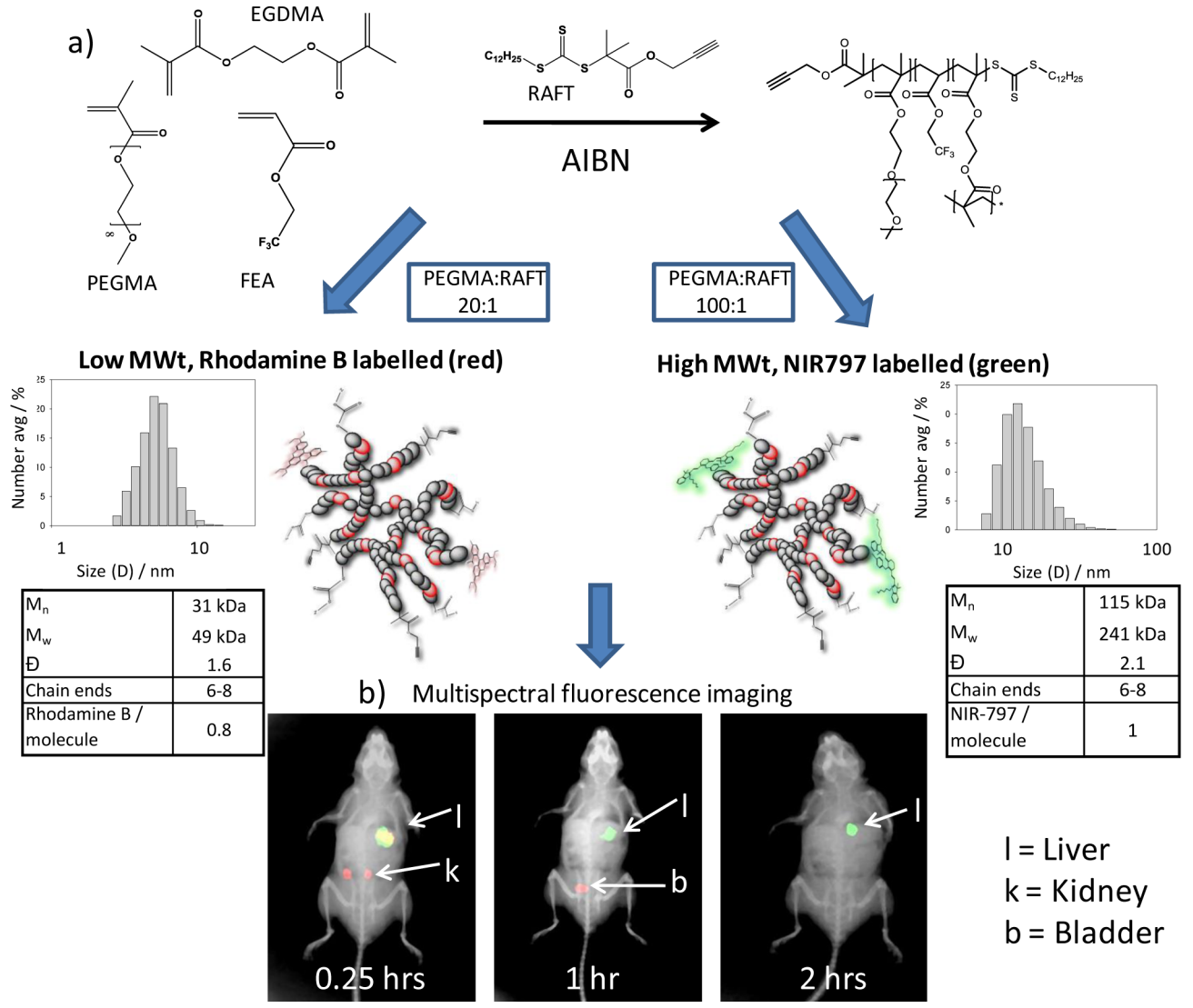

[a](a) General synthetic scheme: synthesis and characterization of various-sized polymeric nanoparticles. (b) Multispectral *in vivo* imaging of two different-sized HBPs (10 mg·mL^{-1} solution of two polymers co-injected into a single mouse) to highlight the effect of molecular characteristics of HBPs on the biodistribution in animals (fluorescence signal false-colored red (polymer with M_n = 31 kDa) and green (polymer with M_n = 115 kDa).

physicochemical properties is required. Synthetic routes that are robust and practical, yet also allow fine control of size, degree of functionality, and tuning of the activity or efficacy of imaging, are also required. Our approach to achieving this degree of control over nanomaterial properties is shown in Scheme 1, whereby the molecular structure and size are controlled by utilizing reversible addition/fragmentation chain-transfer (RAFT) polymerization,[16] while the end-groups are modified using standard coupling chemistries.[10,17]

Imaging agents based on ^{19}F MRI offer a means to detect diseases in deep tissue where the image is not confounded by background signal since there is minimal endogenous fluorine in the body. Various recent publications have shown the potential of imaging using ^{19}F probes.[18−23] However, requirements for polymeric materials suitable for *in vivo* ^{19}F detection are demanding.[24,25] Importantly, the fluorinated segments must maintain high segmental mobility in order to achieve transverse relaxation times (^{19}F T_2 relaxation times) of sufficient length to permit imaging by standard spin echo or gradient echo pulse sequences.[25−27] This can be achieved by implementing strategies that prevent the very strong fluorine−fluorine interactions that typically occur in solution for these molecules. Utilizing a branched polymeric structure coupled with random incorporation of trifluoroethyl acrylate within a hydrophilic PEG-based macrostructure means that the fluoro segments are always in a hydrated state and maintain extensive segmental mobility. Indeed, the high mobility of the trifluoroethyl acrylate units within this HBP suggests random incorporation of the respective monomer units, since numerous previous reports have shown that tapered or block copolymers lead to significant aggregation of the fluoro segments and subsequent decreased mobility.[26,27] Thus, imaging of the ^{19}F nuclei is possible, even in an aqueous environment with up to 20 mol% of fluoro monomer. The macromolecular conformation of the polymeric system is also important for molecular imaging agents. In contrast to micellar-based systems where the spherical structure may not be maintained at low concentration or under high shear,[28] HBPs impart shape persistence to the macromolecule,

dx.doi.org/10.1021/ja410351h | J. Am. Chem. Soc. 2014, 136, 2413−2419

Scheme 2. Schematic Representation of Hyperbranched Polymer Used in Folate-Targeting Experiments Described in This Report[a]

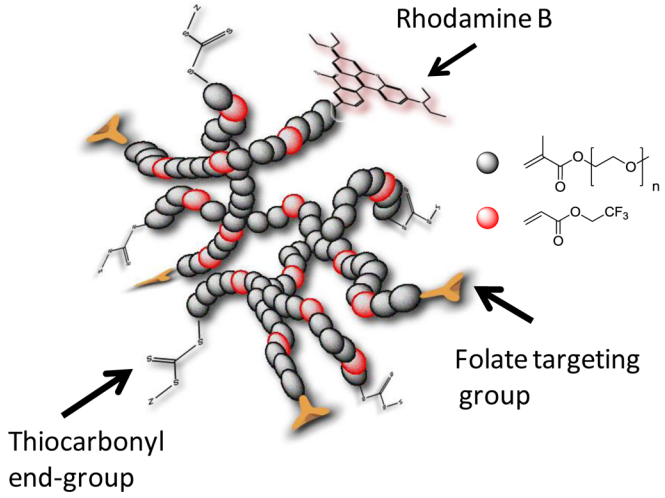

M_n / kDa	31
M_w / kDa	49
$Đ_M$	1.6
R_H / nm (DLS)	4.8
No. Chain Ends	6-8
Folate/molecule	2.5
RITC/molecule	0.8
mol% fluoromonomer	19%

[a]Folic acid is attached via carbodiimide chemistry, while Rhodamine B is conjugated using isothiocyanate chemistry (RITC). The physicochemical properties of the HBP are provided in the inset table.

and the globular nanoparticulate structure is maintained in solution. The use of RAFT chemistry in the synthesis of the polymers imparts a further advantage: all polymer chains (or arms of the HBP) have well-defined end-groups,[29−31] which can be further functionalized with targeting ligands, fluorescent chromophores, or therapeutic drugs. The flexible polymer architecture and ability to position functional groups using a controlled methodology for designing the polymer facilitate an additional level of control over the effective presentation of targeting ligands to receptor proteins on cell surfaces.

We report here the design, synthesis, and implementation of a new polymer-based multimodal imaging platform, incorporating two highly sensitive imaging modalities (fluorescence and ^{19}F MRI) together with cellular-targeting capabilities (folate ligands) in a single nanoparticle. By taking advantage of the respective modalities, it is possible to perform confocal fluorescence imaging of individual cells *in vitro* and also use ^{19}F MRI (in conjunction with standard ^{1}H MRI) and fluorescence imaging to detect the materials *in vivo*. To establish the versatility of this multimodal imaging agent, we demonstrate that the folate-labeled polymer is taken up by B16 melanoma cells *in vitro* and targets tumors *in vivo*—this is accomplished through selective targeting using a well-characterized biological test-bed (folate-receptor targeting).[32] The synthetic approach allows facile access to nanoparticles of controllable size, varied core and shell functionality, sensitivity of MRI and optical response, and tuning of biodistribution. We establish the key features of the multimodal nanoparticles through chemical characterization, MRI and optical response *in vitro*, and combined orthogonal sensing performance *in vivo*.

RESULTS AND DISCUSSION

Controlling the various physical and chemical properties of polymers for nanomedicine is of paramount importance when engineering such materials. Factors such as size, shape, conformation, surface functionality, and rigidity can all play roles in affecting biodistribution, pharmacokinetics, and internalization.[33] The synthetic approach toward development of HBPs utilized in this report allows us to modulate these properties in our system, as shown in Scheme 1. The synthesis of HBPs with different hydrodynamic radii in aqueous solution was confirmed by light-scattering techniques, while multispectral fluorescence imaging (Rhodamine B and NIR-797) delineated the different biodistribution and pharmacokinetics of the two different-sized polymers in a mouse model. Clearly, control over the size of the nanoparticle affords the ability to exert some control over biodistribution and pharmakokinetics of the polymer, with fast clearance of HBPs having sizes of ∼7−8 nm (no detectable signal 2 h following i.v. injection of the polymer solution) and prolonged circulation for polymers of size >11 nm (accumulated signal in liver remaining after 2 h post-injection).

Confirmation of the success of the synthetic strategy was afforded via absolute molecular weight determination of the polymers using multiangle laser light scattering (MALLS) and size exclusion chromatography (SEC). Both the molar mass and the hydrodynamic radius (measured by dynamic light scattering) were relatively low for these molecules compared to other polymeric drug delivery systems such as polymer micelles. The molecular control achievable using RAFT polymerization enabled the molecular size of the HBPs to be tuned. We aimed for polymers with molecular sizes such that the particles would either be rapidly excreted through the kidneys unless bound to receptors on a cell surface (Rhodamine B-labeled polymer in Scheme 1; <8 nm) or, in the case of larger molecules, evade renal filtration to prolong circulation time (NIR797-labeled polymer in Scheme 1; >10 nm).[34]

Following demonstration of the ability to control the size of the polymeric particles and their subsequent behavior *in vivo*, we focused on developing an experimental model to demonstrate both the sensitivity of the imaging agents ands the efficacy of receptor binding. This required postfunctionalization of the nanoparticle with targeting ligands. The number of chain ends on the polymeric nanoparticle was calculated by comparing the molar mass determined by ^{1}H NMR with the absolute molar mass by SEC-MALLS. ^{1}H NMR provides information on the relative chain length in the absence of branching since, according to RAFT theory, each polymer chain will be terminated with either a thiocarbonylthio moiety or the so-called "leaving" group from the original RAFT agent, which

dx.doi.org/10.1021/ja410351h | J. Am. Chem. Soc. 2014, 136, 2413−2419

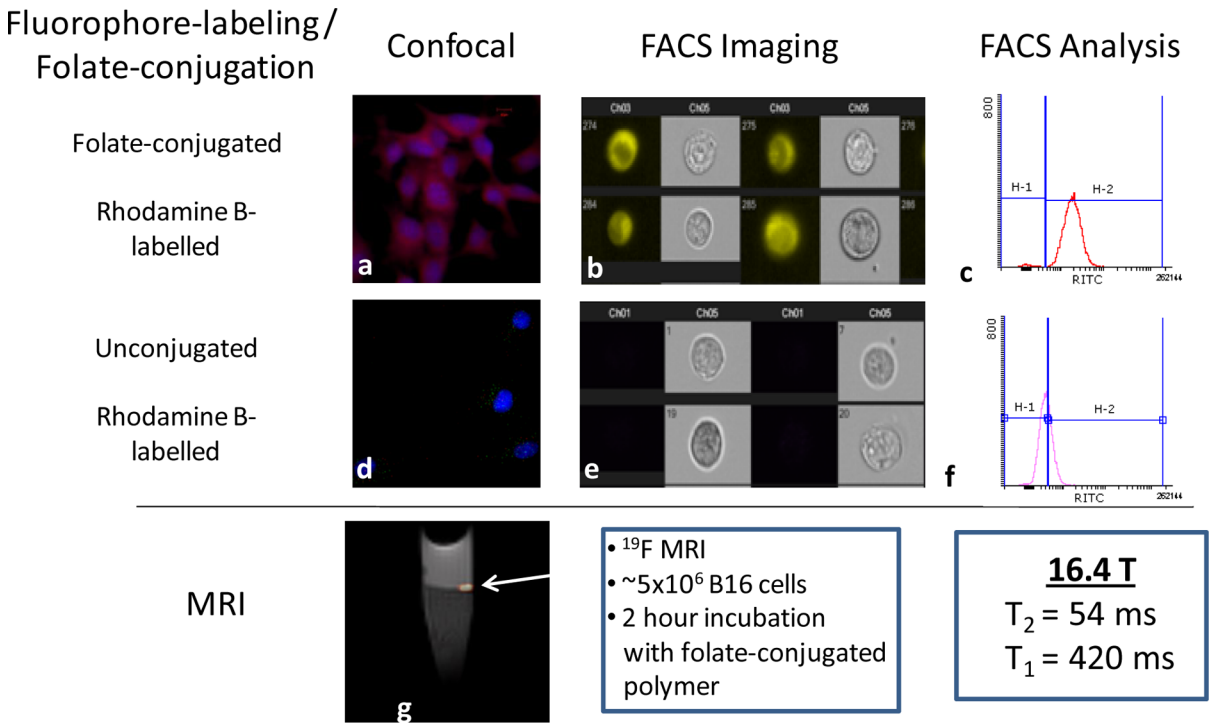

Figure 1. Comparison of cellular uptake data of folate-conjugated and unconjugated HBPs: (a,d) confocal microscopy, (b,e) FACS imaging, and (c,f) FACS analysis for folate-conjugated (a–c) and unconjugated (d–f) B16 cells, respectively. Nuclei were stained with Hoechst 33358, while polymer was labeled in all cases with Rhodamine B. (g) ^{19}F image of approximately 5 × 10^6 cells following incubation with folate-conjugated HBP (false color), overlaying the ^{1}H image of the tube of agar. The ^{19}F relaxation times at 16.4 T for folate–HBP conjugate following uptake into B16 melanoma cells are also presented.

in this case incorporates an alkyne group. Similarly, the molar percentage of trifluoroethyl acrylate within the HBP was calculated by comparing the resonances in ^{1}H NMR for each monomer species. Finally, folic acid and/or fluorescent label was attached using copper-catalyzed click chemistry,[17] in which a short PEG chain (α-amino-ω-azide) was first conjugated to the alkyne-terminal chains, followed by reaction with either the acid group of folic acid (using standard carbodiimide coupling) or the reactive isothiocyanate group on Rhodamine B isothiocyanate (RITC). The folic acid was used as a targeting ligand for the FOLRα receptor[32] (as described below), while the RITC was used as a fluorescent marker for both *in vivo* and *in vitro* studies. The number of folate or RITC groups per molecule was determined using UV–vis spectroscopy. A schematic of the nanoparticle highlighting the important components as described in this report is shown in Scheme 2.

Successful imaging using the designed ^{19}F molecular imaging agents relies on the macromolecule maintaining high segmental mobility in solution, both in serum and in intracellular fluid. Serum stability was tested using simulated body fluids, but the greater challenge was to determine whether cellular internalization of the polymer would affect the MRI properties. This is important because it was not known whether polymer mobility (and hence imaging performance) changes with pH or different redox environments that are typically encountered within intracellular compartments.[35,36] In order to design a system that facilitates high molecular uptake, folate receptor-mediated targeting was investigated using B16 melanoma cells, which like many tumor cells have been reported to overexpress the folate receptor (FOLRα).[14] B16 cells were incubated with RITC-labeled HBPs that were used either "as synthesized" (control) or conjugated with folic acid (Figure 1). Confocal microscopy and fluorescence-activated cell sorting (FACS) analysis clearly shows that the presence of folate groups on the polymer increases the rate and degree of molecular import into cells. In contrast, cells showed very little uptake of the control (unconjugated) polymer; this is due to the reported "stealth" properties of pegylated molecules in which the largely hydrophilic HBP shows minimal interaction with the cell membrane.[14,37,38] In addition, a competitive binding assay with free folic acid showed minimal uptake of the folate-conjugated polymer into cells, suggesting that internalization was via a receptor pathway. The full FACS data are provided in Table 1,

Table 1. *In Vitro* Uptake Studies for Hyperbranched Polymers into B16 Mouse Melanoma Cells[a]

	no. of cells (%)	mean fluorescence intensity
nonconjugated HBP	40	190
folate-conjugated HBP	99	2000
folate-conjugated HBP + 0.1 mM free folic acid	23	60

[a]FACS output provides values for 10 000 cells for each system.

where both the number of cells and mean fluorescence intensity of the cells incubated with folate-conjugated polymer are higher than those with nonconjugated polymer. Likewise, the competitive binding assay shows minimal uptake of the folate-conjugated polymer into cells when free folic acid is present in the medium, suggesting that internalization occurs via the folate receptor.

In order to determine whether internalization of the folate–HBP complexes affected their MRI properties, approximately 5 million cells were incubated with folate-conjugated polymer for

dx.doi.org/10.1021/ja410351h | J. Am. Chem. Soc. 2014, 136, 2413–2419

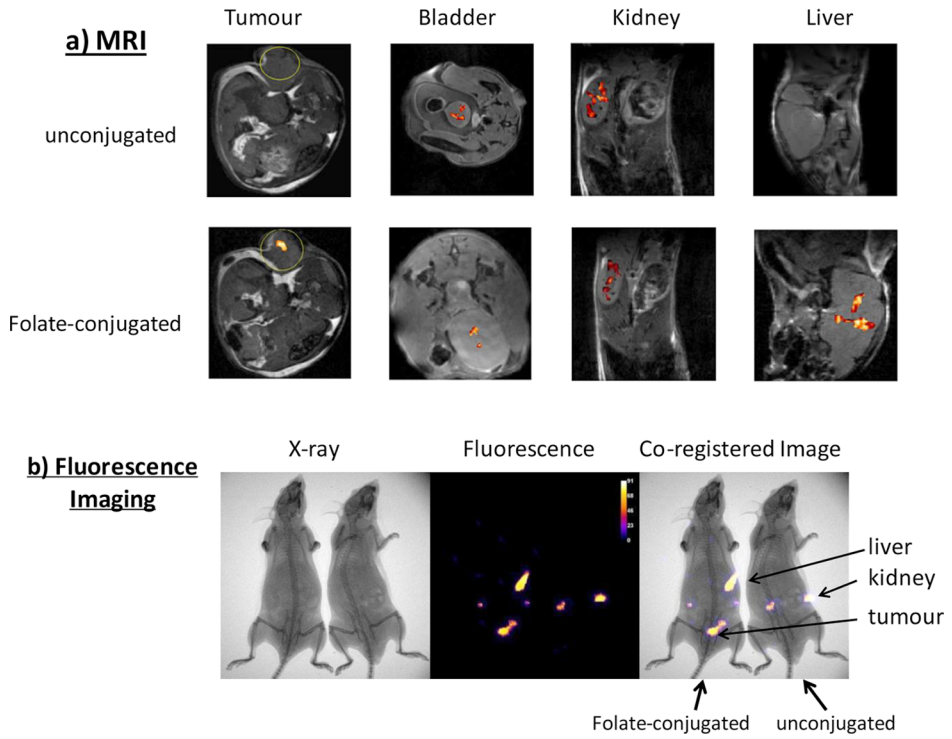

Figure 2. Demonstration of the efficacy of HBP for molecular imaging using the mouse subcutaneous B16 melanoma model. (a) MRI images of bladder, kidney, liver, or tumor (circled in image) in the tumor-bearing mice 1 h following intravenous injection of 100 μL of folate-conjugated or unconjugated (control) HBP (20 mg/mL in PBS). The high-resolution ^{1}H MR image is overlaid with the ^{19}F image. (b) Fluorescence images of mice following injection of the same two compounds at the same concentration. The fluorescence images are co-registered with X-ray images of the mice 1 h following subcutaneous injection.

2 h and then fixed and pelleted by centrifugation. The resulting "pellet" was placed onto an agar bed for imaging. Figure 1g shows the resulting ^{19}F MR image of the cells overlaying the ^{1}H image of the tube containing the water/agar. In this image, the agar and water phases are clearly distinguishable within an Eppendorf tube (grayscale image). The fluorine image is overlaid in color and appears as a pellet sitting on the agar bed, demonstrating that the cells were clearly detected using ^{19}F MRI. Furthermore, the ^{19}F transverse and longitudinal relaxation times (T_2 and T_1, respectively) were measured and found to be within the useful range for preclincial ^{19}F imaging.[24] These results demonstrate the ability to image polymeric agents internalized within isolated cells. They also suggest that this new class of multimodal, polymeric molecular imaging agents may be used to detect tumors *in vivo*.

The incorporation of multiple imaging modalities on a single imaging probe allows the development of more advanced systems, in which the distinct advantages of each imaging modality can be exploited.[7] We have attached a fluorescent probe as an imaging modality complementary to ^{19}F MRI. This dual-modal system combines the sensitivity and relatively low-cost advantages of fluorescence imaging with the high-resolution capabilities of MRI. The fluorescence label also provides a convenient means for *ex vivo* monitoring of cellular uptake of the imaging agent. The major advantage of MRI over other imaging techniques is the very high anatomical resolution that can be achieved.[5] When ^{19}F molecular imaging agents are used, the ^{1}H image can be overlaid with the ^{19}F image, affording exceptional site recognition and anatomic positioning of the molecular imaging agent *in vivo*.[18,23,39] In order to demonstrate the effectiveness of the HBP nanoparticles for molecular imaging, we employed a mouse subcutaneous tumor model (Figure 2).

Both MR and fluorescence images show a clear presence of the folate-conjugated and unconjugated molecular imaging agents in major organs (4 h following i.v. injection of HBPs), highlighting the intrinsic sensitivity and complementarity of these imaging techniques: fluorescence imaging provides whole animal images, allowing tracking of nanoparticles, while ^{19}F MRI provides high-resolution images for analyzing the distribution of nanoparticles within single organs. In the case of this particular experiment, 5 mm slices were utilized to gain maximum signal intensity for elucidation of signal accumulation in particular organs. For future applications, smaller slices will improve the resolution beyond that presented in Figure 2. The nontargeted sample is localized in the bladder and kidney, suggesting that the polymer is small enough to be excreted via the kidneys; accumulation does not appear to occur in the remaining organs to a significant extent. In the case of the folate-targeted polymer, ^{19}F image intensity is observed in the region of the tumor and liver in addition to the kidney and bladder. This is due to the fact that, in addition to being overexpressed on the B16 cells, folate receptors are also expressed by normal tissue within the liver and kidneys.[40] Similar to the ^{19}F MR images, the fluorescence signal from the folate-conjugated polymer is observed in the liver, kidney, bladder, and tumor, whereas that from the unconjugated polymer is seen only in the kidney. The absence of signal in the bladder suggests the animal's bladder was empty at the time of imaging. We do not believe that the signal observed in the liver is due to phagocytosis of particles via the MPS, first because the unconjugated polymer was not detected in the liver, and the addition of folic acid moieties does not significantly alter the

dx.doi.org/10.1021/ja410351h | J. Am. Chem. Soc. 2014, 136, 2413−2419

size or hydrophobicity of the macromolecule, and second because, if the polymer were phagocytosed, we would also expect to see signal within other organs involved in the MPS, including the spleen.[34] Indeed, *ex vivo* fluorescence imaging of organs revealed only minimal detectable signal within the spleen at the time of imaging (Figure 3).

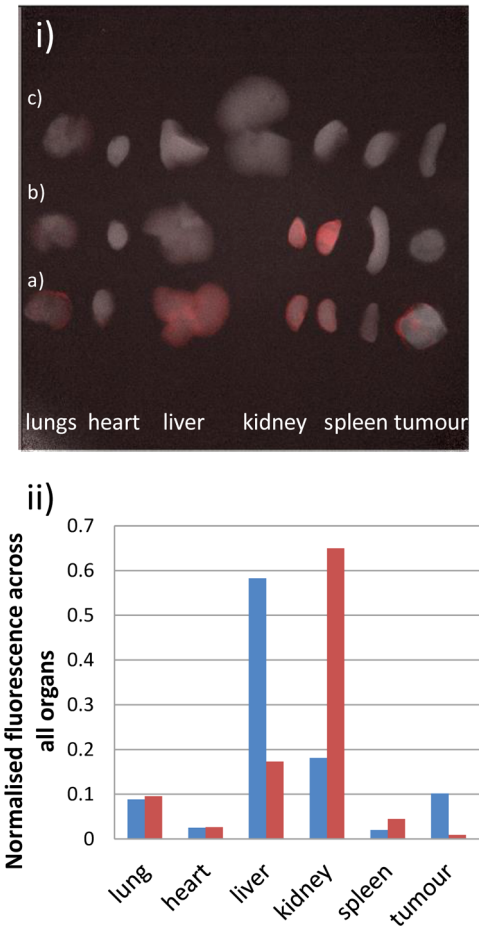

Figure 3. (i) Co-registered X-ray and fluorescence images of excised mouse organs 4 h following i.v. injection of RITC-labeled HBP (50 μL of 20 mg·mL^{-1}): (a) folate-conjugated, (b) non-folate-conjugated, and (c) control images for animal without polymer injection. (ii) Normalized fluorescence intensity throughout excised organs for folate-conjugated (blue) and nonconjugated polymer (red), shown in bar chart.

It is worth noting here that the signal from both the ^{19}F MRI and the fluorescence appears non-homogeneously throughout the tumor and organs. In the case of fluorescence, this can be attributed to absorption of radiated light by tissue. In addition, the B16 melanoma cells have high expression of melanin, which acts as a quencher of fluorescence (even for far-red dyes). For the case of ^{19}F MRI, selected slice geometries and lower sensitivity (compared to fluorescence signal) may be attributed to the concentration of signal in these images. Optimization of acquisition parameters will likely improve the image properties in future experiments. Nonetheless, the *in vivo* imaging successfully showed that accumulation of targeted polymer nanoparticles in tumors could be detected using multiple modalities, and we demonstrate the first example of polymeric agents being used to detect tumors by ^{19}F MRI.

The MRI and *ex vivo* fluorescence data regarding nanoparticle uptake into the tumor were confirmed by FACS analysis of B16 tumor cells following excision and enzymatic digestion (Table 2). The results showed that 39 ± 5% (n = 2) of B16 cells had taken up the intravenously injected folate-conjugated polymer after 4 h, indicating the ability of these particles to both target melanoma cells and be internalized via the folate receptor *in vivo*. The nonconjugated polymer was detected in only 1% of the cells within the tumor under the same experimental conditions. Furthermore, imaging of mice 24 h following i.v. injection of HBPs showed that significant signal from the folate-conjugated polymer was still detectable in both the liver and the tumor by both ^{19}F MRI and fluorescence imaging, while the unconjugated polymer exhibited no detectable signal by either technique. Collectively, this evidence suggests that the molecule is small enough to be excreted via the kidneys and, in the absence of any mechanism for specific cellular uptake (e.g., via the folate receptor-mediated pathway), is rapidly removed from the animal.

Table 2. FACS Data for Single-Cell Suspensions from Excised Organs for Mice, 4 h Following Injection of Folate-Conjugated and Non-Folate-Conjugated HBP[a]

	spleen	tumour
nonconjugated	n/a	1.2% (415)
folate-conjugated	5.4% (700)	39% (800)

[a]Data are averages for n = 2 mice per experiment, and a minimum of 10 000 cells were recorded. Mean fluorescence intensity for each experiment is reported in parentheses.

CONCLUSION

We have developed a materials platform for the synthesis of well-defined polymeric nanoparticles that are highly sensitive molecular imaging agents suitable for detection by both fluorescence imaging and ^{19}F MRI. The robust chemistry allows excellent control over the structure of the hyperbranched molecules, which can be tailored to determine the *in vivo* biodistribution. The flexible synthetic methodology also allows facile postconjugation of cell-targeting ligands such as folate for effective detection of tumors. This versatile approach provides a powerful platform technology for advanced multimodal imaging devices for *in vivo* detection of multiple diseases, combining the high resolution of ^{19}F MRI and the sensitivity of optical imaging.

ASSOCIATED CONTENT

Supporting Information

Full experimental procedures. This material is available free of charge via the Internet at http://pubs.acs.org.

AUTHOR INFORMATION

Corresponding Author

k.thurecht@uq.edu.au

Notes

The authors declare no competing financial interest.

ACKNOWLEDGMENTS

The authors acknowledge the Australian Research Council for funding (FT110100284 (K.J.T.), FT100100721 (I.B.), DP1094205 (I.B., K.J.T.), and DP110104299 (A.K.W.)). We

acknowledge Dr. Nyoman Kurniawan for assistance with MRI, and the Australian National Fabrication Facility QLD-node for characterization assistance. Mr Joshua McHattan from Bruker is gratefully acknowledged for his advice in optical imaging.

REFERENCES

(1) Kelkar, S. S.; Reineke, T. M. *Bioconjugagte Chem.* **2011**, *22*, 1879.
(2) Kircher, M. F.; Hricak, H.; Larson, S. M. *Mol. Oncol.* **2012**, *6*, 182.
(3) Bardhan, R.; Chen, W.; Bartels, M.; Perez-Torres, C.; Botero, M. F.; McAninch, R. W.; Contreras, A.; Schiff, R.; Pautler, R. G.; Halas, N. J.; Joshi, A. *Nano Lett.* **2010**, *10*, 4920.
(4) Cheon, J.; Lee, J.-H. *Acc. Chem. Res.* **2008**, *41*, 1630.
(5) Huang, W.-Y.; Davis, J. J. *Dalton Trans.* **2011**, *40*, 6087.
(6) Boase, N. R. B.; Blakey, I.; Thurecht, K. J. *Polym. Chem.* **2012**, *3*, 1384.
(7) Thurecht, K. J. *Macromol. Chem. Phys.* **2012**, *213*, 2567.
(8) Maeda, H. *Bioconjugate Chem.* **2010**, *21*, 797.
(9) Achilefu, S. *Chem. Rev.* **2010**, *110*, 2575.
(10) Hawker, C. J.; Wooley, K. L. *Science* **2005**, *309*, 1200.
(11) Devonport, W.; Hawker, C. J. *Polym. News* **1996**, *21*, 370.
(12) Fréchet, J. M. J.; Hawker, C. J. *Comprehensive Polymer Science*, 2nd Suppl.; Pergamon: Oxford, UK, 1996; p 71.
(13) England, R. M.; Rimmer, S. *Polym. Chem.* **2010**, *1*, 1533.
(14) Knop, K.; Hoogenboom, R.; Fischer, D.; Schubert, U. S. *Angew. Chem., Int. Ed.* **2010**, *49*, 6288.
(15) Veronese, F. M.; Pasut, G. *Drug Discovery Today* **2005**, *10*, 1451.
(16) Chiefari, J.; Chong, Y. K.; Ercole, F.; Krstina, J.; Jeffery, J.; Le, T. P. T.; Mayadunne, R. T. A.; Meijs, G. F.; Moad, C. L.; Moad, G.; Rizzardo, E.; Thang, S. H. *Macromolecules* **1998**, *31*, 5559.
(17) Rostovtsev, V. V.; Green, L. G.; Fokin, V. V.; Sharpless, K. B. *Angew. Chem., Int. Ed.* **2002**, *41*, 2596.
(18) Ahrens, E. T.; Flores, R.; Xu, H.; Morel, P. A. *Nat. Biotechnol.* **2005**, *23*, 983.
(19) Srinivas, M.; Boehm-Sturm, P.; Figdor, C. G.; de Vries, I. J.; Hoehn, M. *Biomaterials* **2012**, *33*, 8830.
(20) Bonetto, F.; Srinivas, M.; Heerschap, A.; Mailliard, R.; Ahrens, E. T.; Figdor, C. G.; de Vries, I. J. M. *Int. J. Cancer* **2011**, *129*, 365.
(21) Ruiz-Cabello, J.; Barnett, B. P.; Bottomley, P. A.; Bulte, J. W. M. *NMR Biomed.* **2011**, *24*, 114.
(22) Srinivas, M.; Heerschap, A.; Ahrens, E. T.; Figdor, C. G.; de Vries, I. J. M. *Trends Biotechnol.* **2010**, *28*, 363.
(23) Janjic, J. M.; Srinivas, M.; Kadayakkara, D. K. K.; Ahrens, E. T. *J. Am. Chem. Soc.* **2008**, *130*, 2832.
(24) Thurecht, K. J.; Blakey, I.; Peng, H.; Squires, O.; Hsu, S.; Alexander, C.; Whittaker, A. K. *J. Am. Chem. Soc.* **2010**, *132*, 5336.
(25) Du, W.; Nystrom, A. M.; Zhang, L.; Powell, K. T.; Li, Y.; Cheng, C.; Wickline, S. A.; Wooley, K. L. *Biomacromolecules* **2008**, *9*, 2826.
(26) Peng, H.; Blakey, I.; Dargaville, B.; Rasoul, F.; Rose, S.; Whittaker, A. K. *Biomacromolecules* **2009**, *10*, 374.
(27) Nystrom, A. M.; Bartels, J. W.; Du, W.; Wooley, K. L. *J. Polym. Sci., Part A: Polym. Chem.* **2009**, *47*, 1023.
(28) Owen, S. C.; Chan, D. P. Y.; Shoichet, M. S. *Nano Today* **2012**, *7*, 53.
(29) Barner-Kowollik, C.; Blinco, J. P.; Destarac, M.; Thurecht, K. J.; Perrier, S. Reversible Addition Fragmentation Chain Transfer (RAFT) Polymerization: Mechanism, Process and Applications. In *Encyclopedia of Radicals in Chemistry, Biology and Materials*; Chatgilialoglu, C., Studer, A., Eds.; Wiley: Hoboken, NJ, 2012; p 1895
(30) Tan, J. H.; McMillan, N. A. J.; Payne, E.; Alexander, C.; Heath, F.; Whittaker, A. K.; Thurecht, K. J. *J. Polym. Sci., Part A: Polym. Chem.* **2012**, *50*, 2585.
(31) Munnemann, K.; Kolzer, M.; Blakey, I.; Whittaker Andrew, K.; Thurecht Kristofer, J. *Chem. Commun.* **2012**, *48*, 1583.
(32) Elnakat, H.; Ratnam, M. *Adv. Drug Delivery Rev.* **2004**, *56*, 1067.
(33) Yan, Y.; Such, G. K.; Johnston, A. P. R.; Best, J. P.; Caruso, F. *ACS Nano* **2012**, *6*, 3663.
(34) Moghimi, S. M.; Hunter, A. C.; Murray, J. C. *Pharmacol. Rev.* **2001**, *53*, 283.
(35) Carmeliet, P.; Jain, R. K. *Nature* **2011**, *473*, 298.
(36) Jain, R. K. *Adv. Drug Delivery Rev.* **2012**, *64*, 353.
(37) Patil, A.; Shaikh, I. M.; Kadam, V. J.; Jadhav, K. R. *Curr. Nanosci.* **2009**, *5*, 141.
(38) Huynh, N. T.; Roger, E.; Lautram, N.; Benoit, J.-P.; Passirani, C. *Nanomedicine* **2010**, *5*, 1415.
(39) Srinivas, M.; Turner, M. S.; Janjic, J. M.; Morel, P. A.; Laidlaw, D. H.; Ahrens, E. T. *Magn. Reson. Med.* **2009**, *62*, 747.
(40) Parker, N.; Turk, M. J.; Westrick, E.; Lewis, J. D.; Low, P. S.; Leamon, C. P. *Anal. Biochem.* **2005**, *338*, 284.